Hindawi
International Journal of Antennas and Propagation
Volume 2024, Article ID 3153057, 12 pages
https://doi.org/10.1155/2024/3153057

Research Article

A Compact Highly Isolated Four-Element Antenna System for Ultra-Wideband Applications

V. Prithivirajan,[1] **Mariya Princy Antony Saviour**,[2] **J. Seetha**,[3] **B. Siva Kumar Reddy**,[4] **Anand Anbalagan**,[5] **and D. Rajesh Kumar**[1]

[1]*Department of Electronics and Communication Engineering, Vel Tech Rangarajan Dr. Sagunthala R&D Institute of Science and Technology, Chennai, India*
[2]*Department of Electronics and Communication Engineering, St. Joseph College of Engineering, Chennai, India*
[3]*Department of Electronics and Communication Engineering, Panimalar Engineering College, Chennai, India*
[4]*Department of Electronics and Communication Engineering, CMR Engineering College, Hyderabad, India*
[5]*Department of Electronics and Communication Engineering, Technical Vocational Training Institute, Addis Ababa, Ethiopia*

Correspondence should be addressed to Anand Anbalagan; anand.anbalagan@ftveti.edu.et

Received 11 July 2023; Revised 6 October 2023; Accepted 26 February 2024; Published 20 March 2024

Academic Editor: Amrindra Pal

A small, orthogonally polarized, ultra-wideband (UWB), four-port multiple-input multiple-output (MIMO) printed antenna is presented in this study. The envisioned antenna is built up of four microstrip fractal-based circular patch elements, each of which is fed by a microstrip line with a 50-ohm impedance. The use of a defective ground plane allows for the ultra-wideband frequency response to be obtained. In order to achieve maximal isolation, the amount of surface current that flow between the antenna's four components is limited by arranging radiating elements orthogonally. The four-port MIMO system is printed on a FR4 substrate with a loss tangent of 0.02 and an overall dimension of $20 \times 30 \times 1.6\ mm^3$. A port-to-port isolation of less than 25 dB was achieved as a consequence of this orthogonal orientation of antenna elements, and the impedance bandwidth is achieved up to 158% (3.1–12 GHz). The suggested ultra-wideband multiple-input multiple-output (UWB-MIMO) antenna achieved a maximum gain of 8 dBi over the operational frequency range (3.1–12 GHz); the findings that were measured and those that were simulated accord with one another rather well. The findings also give an overall strong diversity performance, with the ECC < 0.25, DG > 9.9, and CCL < 0.2 values all being within acceptable ranges.

1. Introduction

These days, there is a great deal of demand for needs and requirements that include flow of data without interference. A radio link's capacity may be increased using the multiple-input multiple-output (MIMO) technology by utilising several transmit and receive antennas to accomplish multipath propagation [1]. The deployment of multiple-input multiple-output (MIMO) systems has revolutionized wireless communication networks by significantly enhancing data throughput and spectral efficiency [2]. By exploiting spatial diversity and multiplexing gains, MIMO technology enables simultaneous transmission of multiple data streams over the same frequency band, thereby increasing the overall system capacity. In practical implementations, the effectiveness of MIMO systems heavily relies on the spatial separation of antennas and the mitigation of interference effects. To achieve optimal performance, antennas need to be strategically positioned to maximize diversity and minimize correlation between antenna elements [3, 4]. This spatial arrangement is crucial for combating multipath fading and improving signal quality, especially in environments with severe channel conditions. Ultra-wideband (UWB) technology complements the capabilities of MIMO systems by offering enhanced data rates, low power consumption, and robust communication links. Operating across a wide range

of frequencies, UWB enables high-speed data transmission while adhering to stringent regulatory constraints set by organizations like the Federal Communication Commission (FCC) [5]. The adoption of UWB further extends the applicability of MIMO systems in diverse wireless environments, ranging from personal area networks to industrial IoT deployments. However, the integration of MIMO and UWB technologies introduces challenges associated with antenna design and mutual coupling effects. In compact MIMO antenna configurations, the proximity of antenna elements can lead to mutual coupling, where electromagnetic fields from one antenna influence the performance of neighbouring antennas. Mutual coupling not only degrades the isolation between antenna elements but also affects the radiation pattern and impedance matching of the overall antenna array [6].

Addressing mutual coupling issues is essential for ensuring the robustness and reliability of MIMO-UWB systems, especially in scenarios where signal integrity is paramount. Techniques such as antenna decoupling, isolation enhancement, and adaptive array processing play a pivotal role in mitigating the adverse effects of mutual coupling and optimizing system performance. As we transition into the era of 5G connectivity, the demand for high-speed data transmission, ultra-low latency, and seamless connectivity continues to escalate. MIMO-UWB systems offer a compelling solution to meet these evolving demands by leveraging advanced signal processing algorithms, beamforming techniques, and interference mitigation strategies [7]. This is because radiations from free space, surface currents, and surface waves can all contribute to the formation of mutual coupling. It is possible for the total active reflection coefficient of a MIMO antenna to be altered by a variety of signal processing methods. These techniques include those that reduce carrier frequency offset (CFO), channel estimate, and angle of arrival estimation. When mutual coupling is present, it is possible for large out-of-band (OOB) emissions from power amplifiers (PAs) to interfere with communication on neighbouring channels. In the realm of digital communications, the mutual coupling has been reduced due to improvements made to MIMO precoding and decoding techniques [8]. Before adaptive algorithms can calculate the weight vector, the received voltages must first be adjusted to eliminate any mutual coupling that may have occurred. During postprocessing, one may improve the signal-to-interference noise ratio (SINR) by reducing the amount of relative interference or noise. In order to maintain the SINR, it is not essential to adjust the electromagnetic interactions. Using the approach described above, it is possible to achieve some degree of success in enhancing the electromagnetic suppression in the digital realm. When viewed from the point of view of the antenna, a technology that is efficient in decoupling is more successful at mitigating the consequences of mutual coupling. As a direct consequence of this, approaches for decoupling based on antennas need to be developed [9].

There are a variety of approaches that may be used to achieve decoupling. Examples of such decoupling methods include things like deflected ground structures [10], decoupling networks [11], electromagnetic band gap structures (EBG) [12], neutralising lines [13], parasitic or slot components [14], and complementary split-ring resonator (CSRR) [15]. There is a description of a UWB-MIMO antenna with twin ports in reference [16]. This antenna has wideband features, including a frequency range of 3.0–11.0 GHz as well as four rejection bands. According to the findings presented in reference [17], slots with inverted L and U forms are able to give quadruple notch characteristics at frequencies of 3.3 GHz, 4.03 GHz, and 5.4 GHz. In addition to this, the antenna has an isolation of more than 25 decibels. In [18], a flexible CPW-fed MIMO antenna is shown; in order to achieve strong polarization diversity, a large impedance width of 125.83%, a maximum gain of 6.8 dBi, and an efficiency of 89%, four identical elements are stacked symmetrically in a sequential rotating fashion. This allows the antenna to fulfil its goals. The authors of [19] were able to reduce the size of a UWB-MIMO antenna by combining the radiation from a rhombic slot with that of four microstrip feeders. In order to achieve the notched properties, C-slots, L-slots, and an H-shaped EBG structure must first be opened. The antenna has a strong performance in terms of variety, with an isolation level of 40 dB, a peak gain of 5.5 dBi, and a radiation efficiency range of 75%–90%. In a letter that was cited in [20], it was proven that a wideband impedance match and dual-band notch capability may be achieved by using a quasi-U-shaped patch on the upper plane and a stepped slot in the ground plane. The use of defective ground structure for an elliptical planar antenna has been explored in [21], where the DGS is used to realise a UWB frequency response. The purpose of this study was to investigate the use of DGS. In the research described in [22], two symmetrical half-slot components with CPW-fed structures were used, together with a Y-shaped slot that was split at the bottom centre of the common ground. Both the current flow at low UWB frequency and the mutual coupling between the MIMO components are significantly reduced due to the slots' efficient blocking of both. There is a paper in reference [23] that describes a unique four-element MIMO antenna that may be used for UWB applications; the antenna is CPW-fed and is made up of four orthogonal sections. An impedance width ranging from 2.1 to 20 GHz may be accomplished by using notch frequencies in the range of 3.3 GHz–4.1 GHz and 8.2 GHz–8.6 GHz with the antenna that has been presented. When notches are reached, it is possible to filter out interference from WiMAX and radar applications. In [24], the neutralisation line approach is discussed in relation to its use in the construction of MIMO antennas for UWB communications. The bandwidths that were measured were 95.22% (3.51–9.51 GHz) and 96.47% (3.52–10.0 GHz), and the isolation was improved to 23 dB. The MIMO antenna offers a peak gain of 2.91 dBi and has superior diversity metrics than the other antenna types. In addition, the design of the antenna that is discussed in [25] is for an extremely compact 2-element planar antenna. In order to get the UWB response, a rectangular stepped slot and a z-shaped slot are etched into the ground plane. The described construction has a geometrical dimension of 23 mm by 26 mm by 0.8 mm^3, and the antenna has a peak gain of 5 dBi with an efficiency of 80%.

In this work, we have proposed a fractal-based compact four-element antenna for UWB applications operating from 3 to 12 GHz with high isolation and gain. By placing antenna elements orthogonally, isolation up to 30 dB is achieved which results in lower values of ECC below 0.25. The antenna also achieves maximum gain up to 8 dB which is highly significant for UWB applications. Moreover, MIMO parameters diversity gain (DG) and channel capacity loss (CCL) have also been computed to verify presented MIMO antenna's diverse performance over the operating spectrum. The results show that the antenna proposed in this research could be a viable candidate for UWB applications.

The significance of the proposed work could be stated as follows:

(1) The presented antenna occupies only a minimum area of around $20 \times 30\,\text{mm}^2$ which is relatively smaller in size compared to the other works in the literature.

(2) With such low-profile configuration, the antenna achieves ultra-wideband operation spanning between 3 and 12 GHz with 10 dB impedance bandwidth.

(3) The designed antenna is implemented as a four-element MIMO antenna system which provides high isolation better than 25 dB without seeking additional decoupling mechanism.

(4) Most importantly, the antenna attains maximum gain up to 8 dB which is highly sufficient for UWB applications.

(5) Furthermore, the antenna exhibits considerable MIMO features which include ECC, DG, and CCL over the operating spectrum.

1.1. Single Antenna Design and Analysis. The proposed UWB antenna is illustrated along with its schematic representation as shown in Figures 1(a) and 1(b), respectively. The radiating element of size L × W is printed on front side of 1.6 mm thick (H) FR4 substrate. The radiating element consists of two main components, namely, modified circular patch and feeding strip, as shown in Figure 1(a). To obtain the wide bandwidth, 15 equal steps of size L4 have been etched from the corners of the circular radiating element and connected with a 50-Ω feeding strip of size L1 × W1. On the one hand, defected ground has been printed on the backside of the substrate with the dimension of L1 × W. In order to achieve better impedance matching as well as wider bandwidth, portions of width W3 have been etched away from top of the ground plane. Furthermore, to improve the resonance over the desired band of spectrum, a slot of L3 × W2 has been removed from the centre of the ground plane as shown in Figure 1(b). The detailed dimension of the single antenna element is listed in Table 1.

The reflection coefficient of the proposed UWB antenna is illustrated in Figure 2. It is clearly shown that the proposed antenna is capable of covering UWB spectrum ranging from 3 to 10 GHz over the 10 dB impedance scale.

1.2. Design Process. To provide a better understanding of the proposed design, evolution stages have been studied in this section. The design stages have been categorized as Antenna 1, Antenna 2, Antenna 3, and Proposed Antenna as shown in Figure 3. Antenna 1 consists of full ground plane with a full circle along with feeding strip. Then, Antenna 2 is obtained after reducing the size of ground plane. Ground plane of the Antenna 2 is etched at top left and right edges and named as Antenna 3. The proposed antenna is derived from Antenna 3 by incorporating 15 equal steps over the edges of the circular radiator. The corresponding reflection coefficients are illustrated in Figure 4. Antenna 1 is only able to provide dual and narrow band resonance at 8.5 and 10.25 GHz, respectively. The reduction of ground plane size influences resonance to be created at three spectrums that include 4 GHz, 7.8 GHz, and 10.5 GHz. It proves that defected ground could cause spectrum of operation with reasonable impedance matching. Even better impedance matching with wider spectrum of operation is obtained after making changes along top edges of the ground plane (Antenna 3). The UWB performance is achieved by incorporating fractal-based structure (equal steps) over the circular radiating element as shown in Figure 4.

1.3. Parametric Study. The parametric analysis has been provided in this section to understand the design concepts of the proposed UWB antenna. However, the proposed antenna does have many parameters; only three have been taken for analysis including length of the feed (L1), length of the ground plane (L2), and length of square slot in the ground plane (L3). As shown in Figure 5(a), the parameter L1 has been altered from 10 mm to 13 mm with the equal step size of 1 mm. It is noticed that L1 has influenced wideband resonance while it is progressively increased. The proposed antenna is capable of exhibiting UWB resonance only at 11 mm with significant reflection coefficient below 10 dB. Altering the stub length (L1) results in variations in the frequency of operation. Similarly, the effect of changing ground plane length (L2) is also studied and plotted in Figure 5(b). Increasing length (L2) affects impedance matching of the antenna throughout the bandwidth. On the other hand, variation in slot length (L3) in the ground plane is studied as shown in Figure 5(c). Ground slot length (L3) does not affect the wideband resonance but influences the frequency shift as well as impedance matching of the designed antenna.

1.4. Surface Currents. The antenna surface current distributions at various frequencies are illustrated in Figures 6(a)–6(d). At 4 GHz, current concentration maximizes along the feeding strip as well as in the corners of circular radiating element as shown in Figure 6. It proves that length of the feeding strip affects performance of the antenna at lower frequencies. Figure 5 also shows current distribution at 6 GHz. It is noticed that peak current concentration exists at bottom of the radiating element and sliding edges of the ground plane which influences impedance matching of the

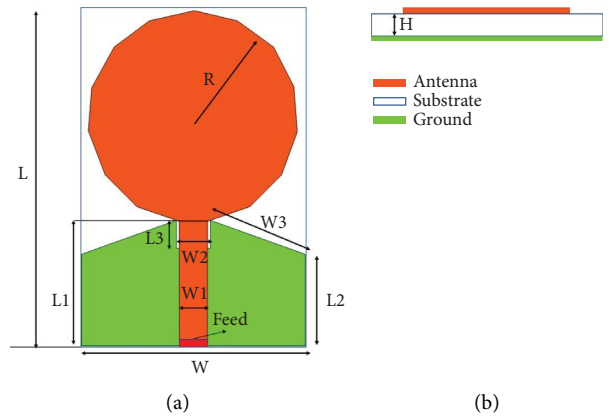

Figure 1: (a) Structure and dimension of single element proposed antenna. (b) Schematic view of the proposed antenna.

Table 1: Various dimensions of the proposed antenna.

Parameters	Values (mm)
L	20
W	30
L1	11
L2	8.0275
L3	2.475
W1	2.5
W2	3
W3	8.4
H	1.6

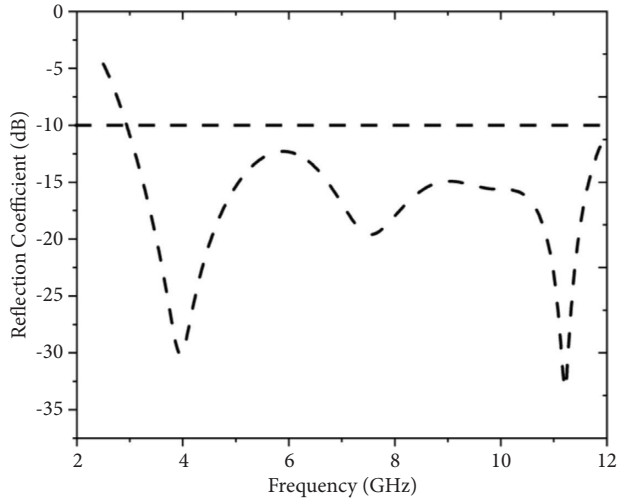

Figure 2: Reflection coefficient of the proposed UWB antenna.

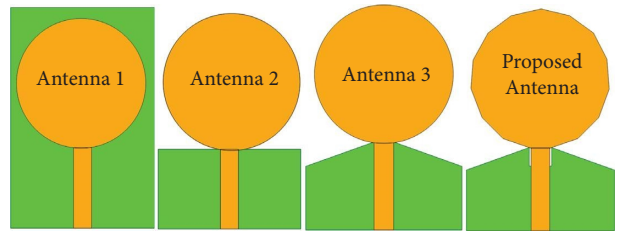

Figure 3: Design stages of the proposed antenna.

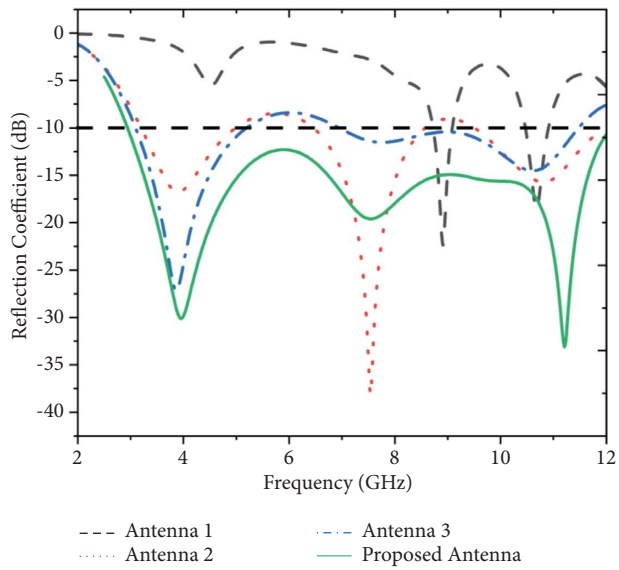

Figure 4: Performance analysis of the proposed antenna during design stages.

antenna at middle range of the spectrum. At 8 GHz, the current concentrated at the edges of the ground slot, whereas at 10 GHz, peak current is observed along the feeding line along with sliding edges on the ground plane as shown in Figure 6.

1.5. MIMO Antenna Structure. The proposed single antenna element is converted into four-port MIMO antenna system which is printed on 65 mm × 65 mm FR4 substrate in orthogonal fashion. All the antenna elements in the MIMO system have covered UWB spectrum ranging from 3 to 12 GHz over the 10 dB impedance scale. Since all the antenna elements are placed orthogonally, significant isolation up to 20 dB is achieved between any adjacent pair. It results in considerable improvement radiation efficiency and envelope correlation coefficient (ECC). The structure of the four-port MIMO antenna is illustrated in Figure 7(a). The fabricated prototype of the MIMO antenna is depicted in Figure 7(b). The simulated and measured reflection and transmission coefficients of the proposed MIMO antenna system are illustrated in Figures 8(a)–8(d). It is observed that both simulated and measured S-parameters of the antenna synchronized well with each other.

It is mentioned earlier that isolation among antenna elements is better than 25 dB as all elements are placed orthogonally. It is verified with surface current distribution of the proposed antenna excited at various frequency of operation as shown in Figures 9(a)–9(c). It is observed that when Antenna 1 is excited, other elements have not been affected by the current which flows in Antenna 1, thereby improving isolation significantly.

Similarly, measured two-dimensional radiation patterns at $\varphi = 0^\circ$ and 90° at 4 GHz, 6 GHz, and 8 GHz are illustrated in Figures 10(a)–10(c). At all the frequency ranges, the proposed antenna exhibits unique pattern over $\varphi = 0^\circ$ and 90° directions with cross-polarization better than 20 dB. The simulated and measured gain of the proposed antenna is illustrated in Figure 11. The proposed MIMO antenna achieves maximum gain up to 8 dBi over the desired operation spectrum which is highly significant for UWB applications. It is noteworthy that any dedicated structure or mechanism has not been included in this work to improve the gain.

1.6. MIMO Performance. In this section, various MIMO features have been discussed to validate the MIMO performance of the proposed antenna. Envelope correlation coefficient is an important parameter which reveals how far antenna elements are displaced, thereby achieving superior performance. Figure 12(a) illustrates the ECC of the proposed antenna which lies in the range between 0.1 and 0.2. The obtained ECCs are lower than the acceptable threshold of 0.5. ECC values of the proposed antenna are calculated using the following equation:

$$\mathrm{ECC}(\rho_e) = \frac{\left| \iint \left[\overrightarrow{A_1}(\Theta, \varphi) \times \overrightarrow{A_2}(\Theta, \varphi)\, d\Omega \right] \right|^2}{\left| \iint \left[\overrightarrow{A_1}(\Theta, \varphi) \right]^2 d\Omega \right| \left| \iint \left[\overrightarrow{A_2}(\Theta, \varphi) \right]^2 d\Omega \right|}. \quad (1)$$

Also, diversity gain of the proposed MIMO antenna system has been computed using (2) and plotted in Figure 12(b). Generally, both DG and ECCs of the antenna are dependent parameters which represent gain of the antenna when radiated wave propagates in diverse directions. Generally, diversity gain of the ideal MIMO antenna system should be 10 dB over the operating spectrum. For the proposed antenna, it is as closer as 9.8 dB between 3 and 10 GHz.

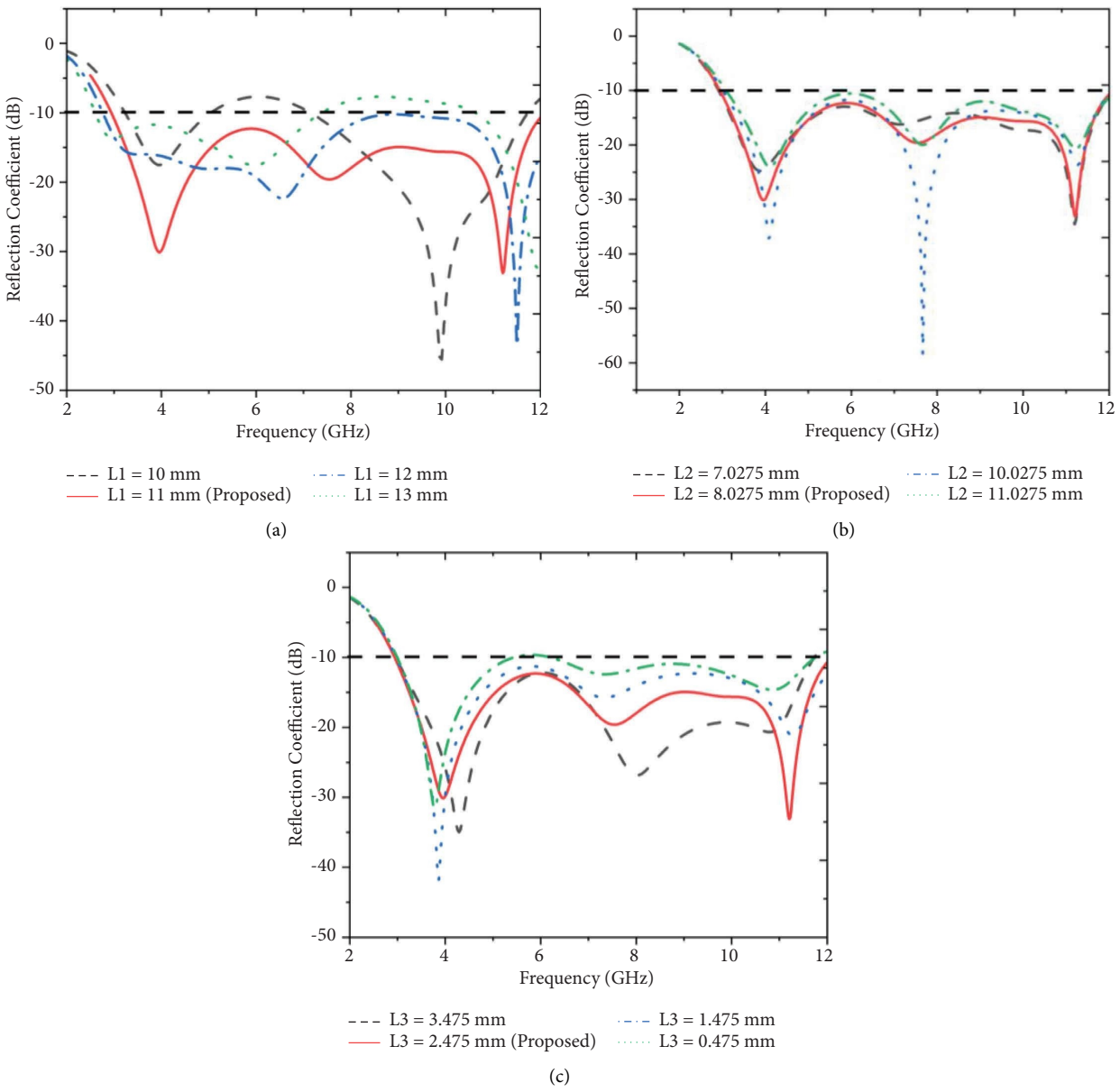

Figure 5: Parametric study of the proposed antenna when altering (a) L1, (b) L2, and (c) L3.

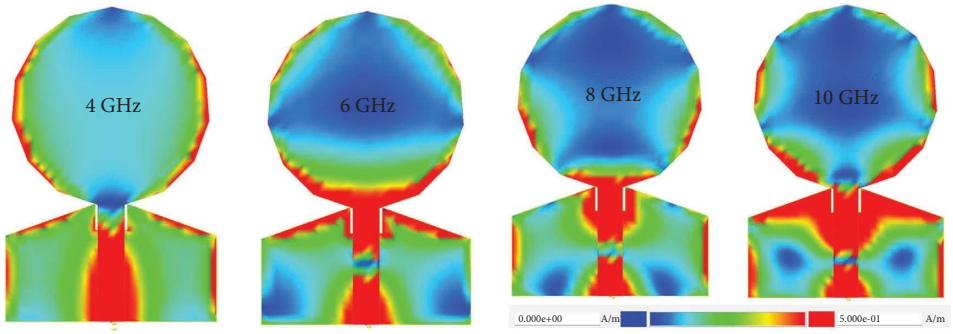

Figure 6: Surface current distribution of the designed antenna.

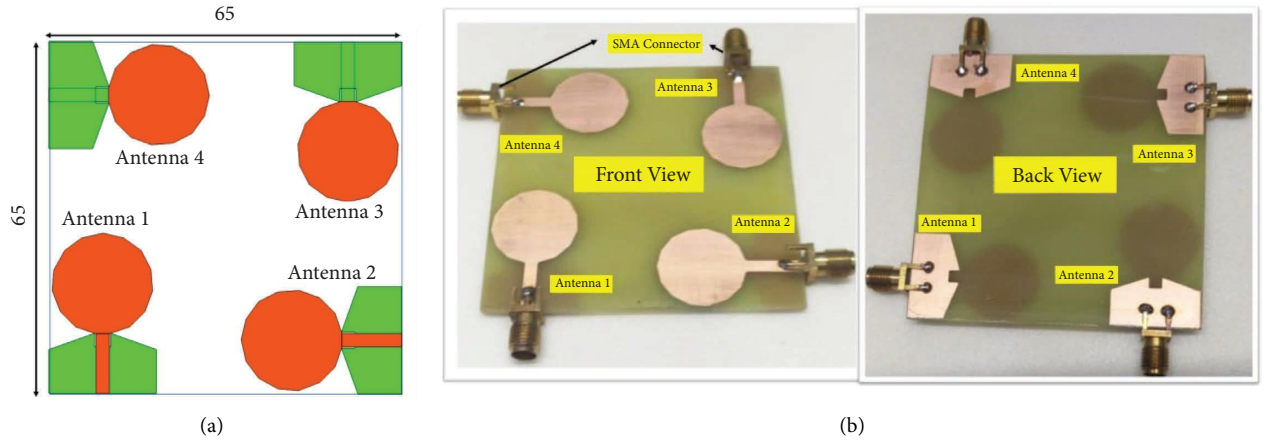

FIGURE 7: (a) Structure of the MIMO antenna. (b) Fabricated images of the proposed antenna.

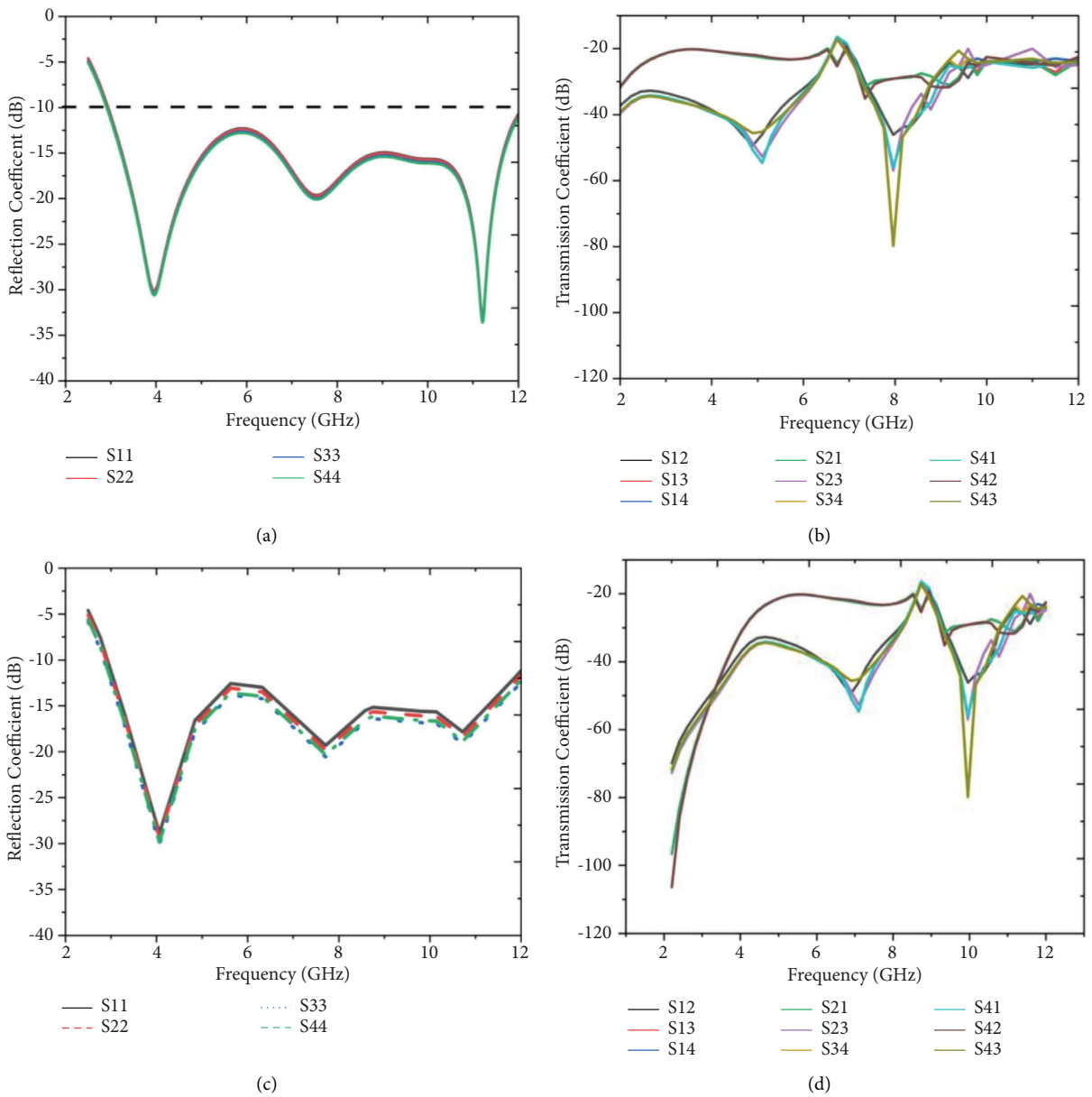

FIGURE 8: Simulated (a) reflection coefficient and (b) transmission coefficient. Measured (c) reflection coefficient and (d) transmission coefficient.

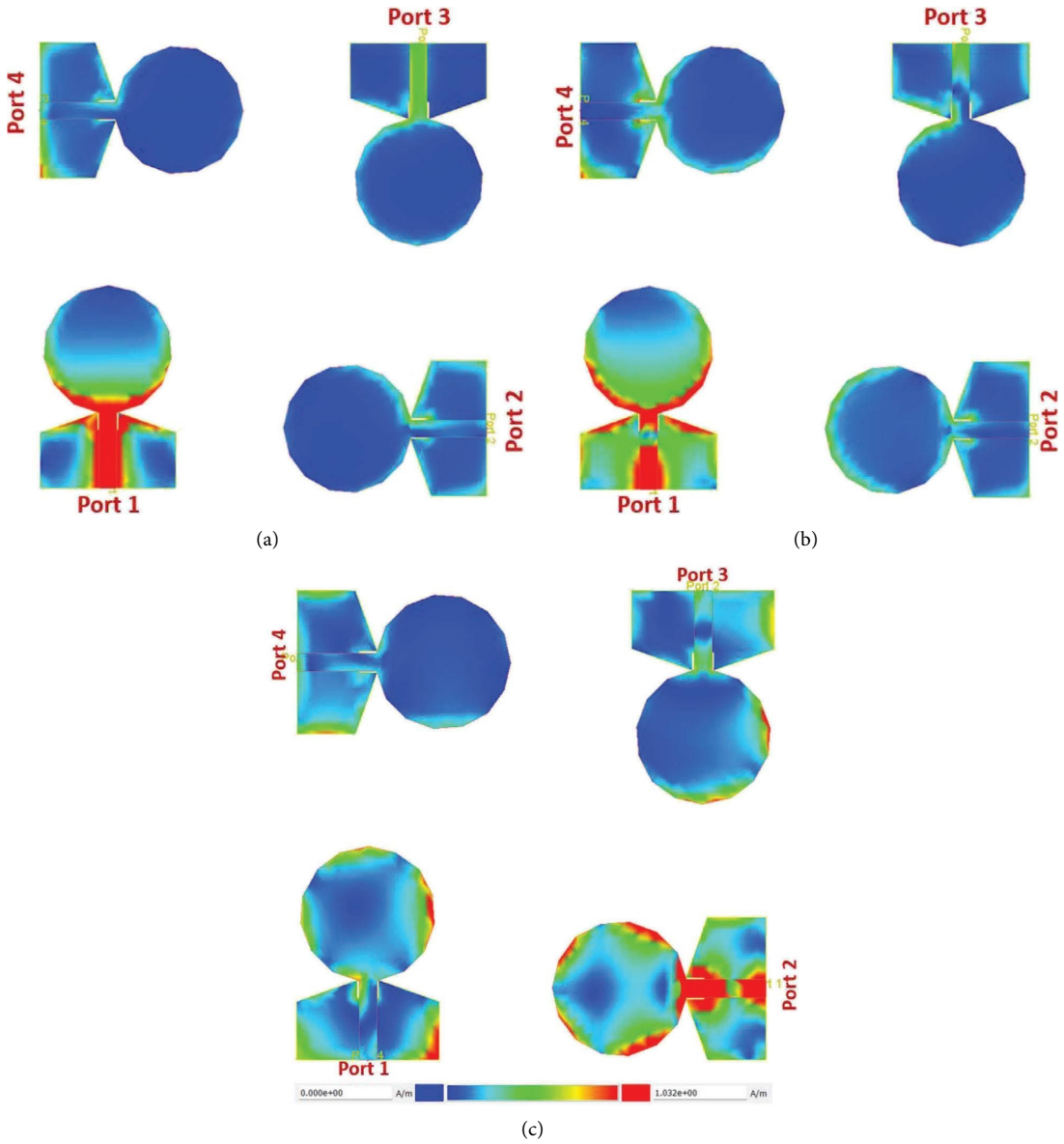

Figure 9: Surface currents of MIMO antenna at (a) 3.5 GHz, (b) 7 GHz, and (c) 9 GHz.

$$\text{Diversity Gain}\,(DG) = \sqrt{1-\rho_e{}^2}. \tag{2}$$

Channel capacity loss (CCL) is an important metric being measured in terms of bits per seconds per Hz using (3) and (4). It measures loss of data during transmission of electromagnetic waves. For ideal antenna system, CCL should be zero but practically it could be less than 0.4 bits/Sec/Hz. The proposed antenna system exhibits CCL around 0.25 bits/Sec/Hz over the operating spectrum as shown in Figure 12(c) that ensures designed antenna has minimum transmission loss during radiation.

$$\text{Channel Loss (CL)} = -\log_2 \det\left(\varphi^{\mathrm{R}}\right), \tag{3}$$

$$\varphi^{R} = \begin{bmatrix} p_{\mathrm{ii}} & \cdots & p_{\mathrm{ij}} \\ \vdots & \ddots & \vdots \\ p_{\mathrm{ji}} & \cdots & p_{\mathrm{jj}} \end{bmatrix}, \tag{4}$$

where

$$\begin{aligned} p_{ii} &= 1 - \left(\left(S_{ii}{}^2\right) + \left(S_{ij}{}^2\right)\right), \\ p_{ij} &= -\left(S_{ii}{}^{*} S_{ij} + S_{ji}{}^{*} S_{jj}\right), \quad \text{for i, j} = 1, 2 \ldots\ldots 4. \end{aligned} \tag{5}$$

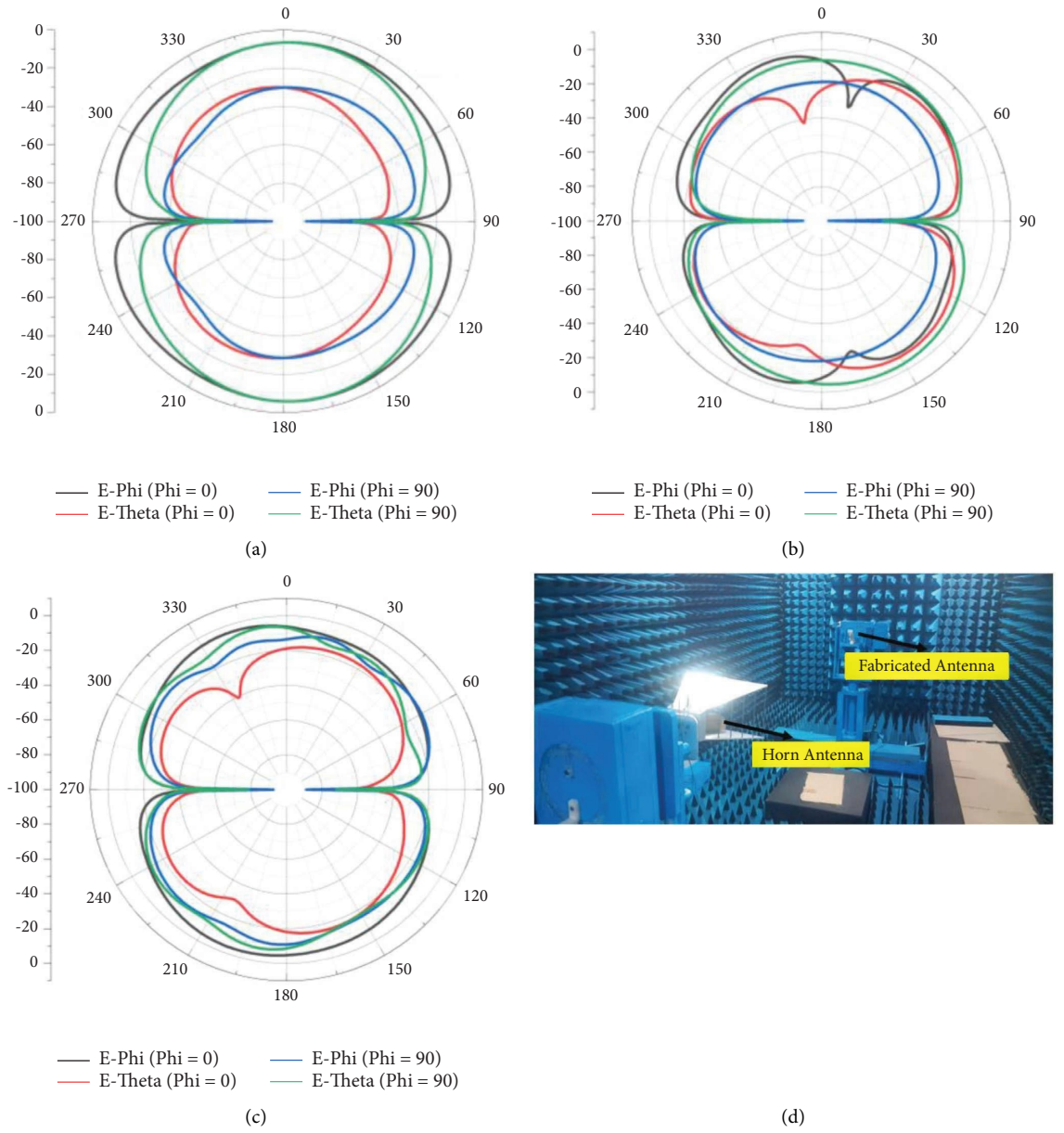

Figure 10: Measured two-dimensional far-field pattern of the proposed antenna at (a) 3.5 GHz, (b) 7 GHz, and (c) 9 GHz. (d) Measurement setup in anechoic chamber.

Figure 13(a) represents total active reflective coefficient of the proposed antenna. It is obvious that TARC will be measured when phase of all ports will be changed when phase of the port 1 is kept constant. It is observed that frequency response of port 1 maintains same bandwidth when altering phase of all other ports. Similarly, multiplexing efficiency has also been calculated and plotted in Figure 13(b). The proposed antenna exhibits multiplexing efficiency lower than 2.8 dB over the operating bandwidth which is within the acceptable limit of the MIMO antenna system. The overall performance of the designed antenna reflects that it could be a suitable candidate for UWB applications.

State-of-the-art comparison is presented in Table 2. It is observed that size of an individual antenna has been comparatively minimized about $20 \times 30\,\text{mm}^2$ with significant gain up to 8 dB. By placing antenna elements orthogonally, the proposed antenna achieves isolation up to 25 dB with significant MIMO parameters including ECC, DG, and CCL.

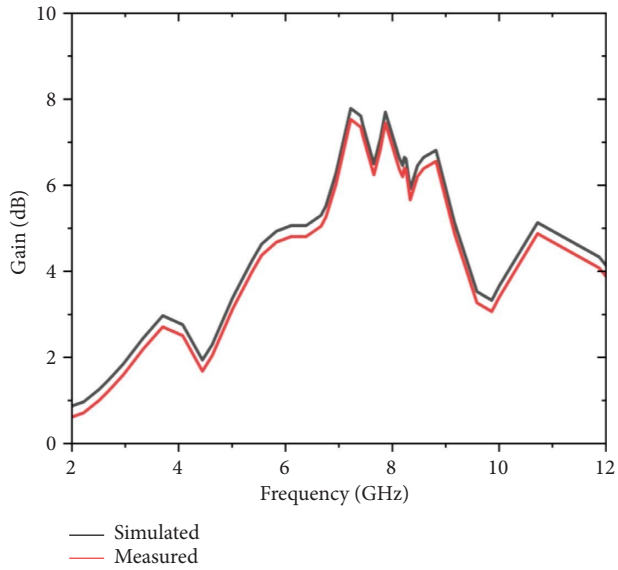

Figure 11: Simulated and measured gain of the proposed antenna.

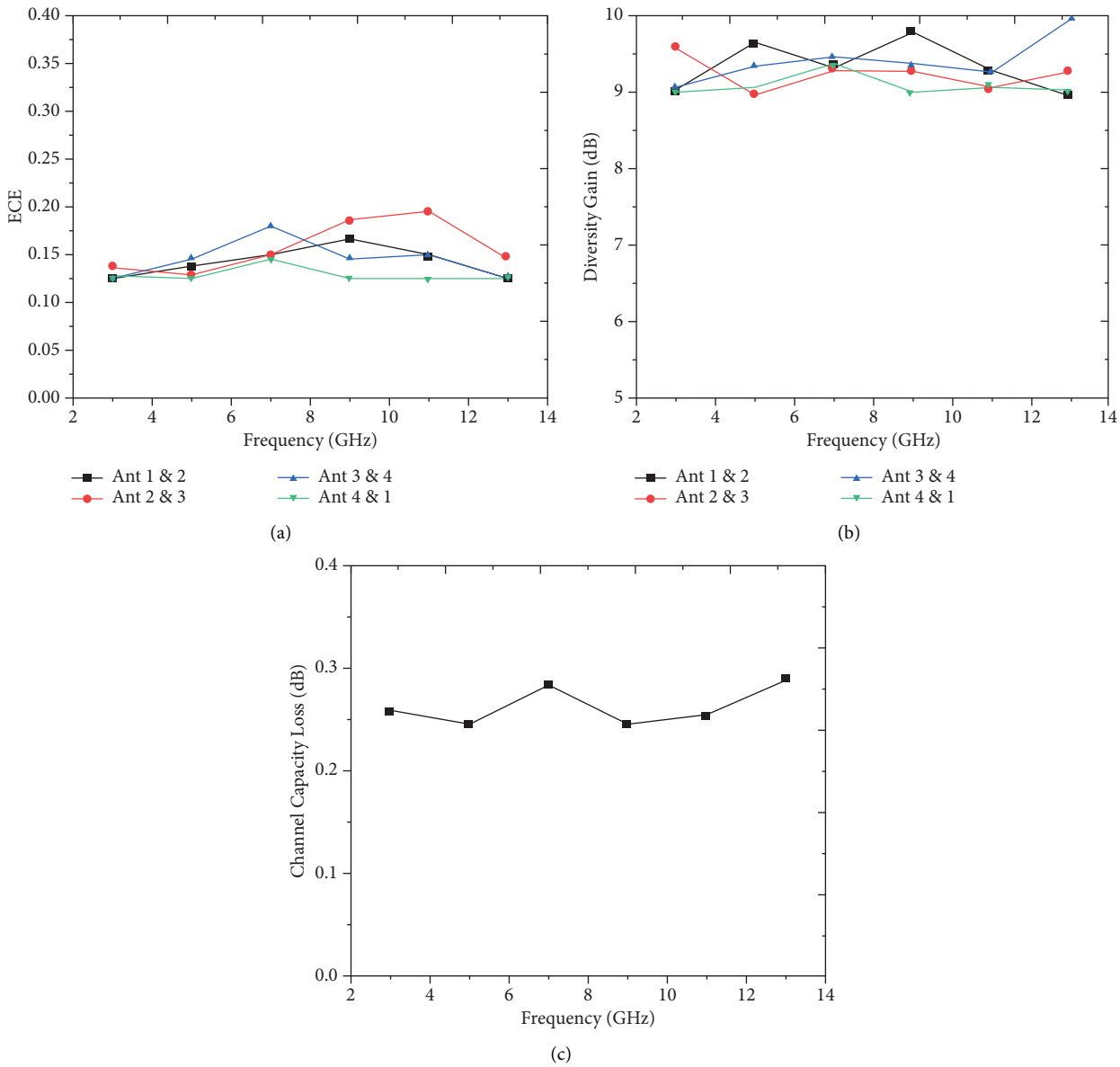

Figure 12: MIMO parameters: (a) ECC, (b) diversity gain, and (c) channel capacity loss.

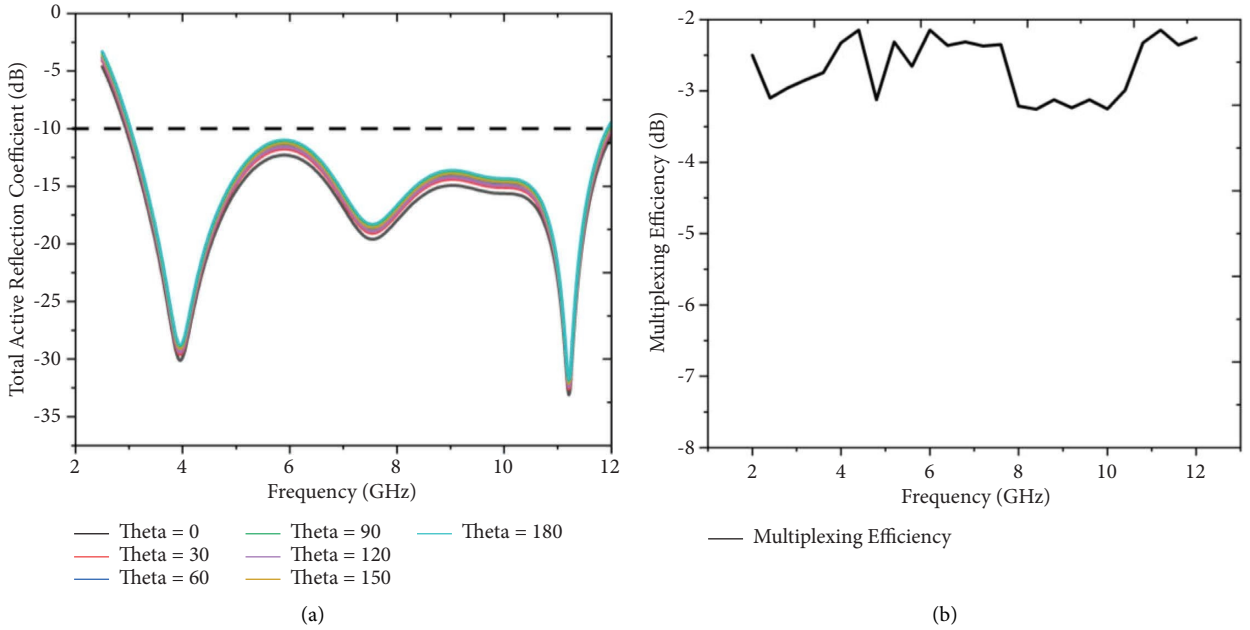

Figure 13: (a) TARC. (b) Multiplexing efficiency of the proposed antenna.

Table 2: State-of-the-art comparison of the proposed antenna with the literature.

Ref. no	Antenna size (mm^2)	Frequency of operation (GHz)	Electrical dimension of the antenna (λ^2)	Isolation (dB)	Max. gain (dB)	ECC	DG	CCL
[9]	56×68	3.89–17.09	$0.726\lambda \times 0.88\lambda$	15	5.87	<0.02	NA	<0.5
[10]	34×34	3.3–3.9, 5-6, 7.4–8.5	$0.374\lambda \times 0.374\lambda$	15	5.5	<0.05	NA	NA
[14]	80×80	3 to 4	$0.8\lambda \times 0.8\lambda$	25	5.8	<0.02	9.9	<0.4
[15]	48×34	2.1–20	$0.336\lambda \times 0.238\lambda$	23	2.91	NA	9.81	<0.29
[17]	74×74	3.37–27.71	$0.831\lambda \times 0.831\lambda$	34	7.68	<0.039	NA	NA
[21]	36×35	2.6–12.2	$0.312\lambda \times 0.303\lambda$	17	NA	NA	9.99	NA
[22]	40×40	2.6–12.2	$0.346\lambda \times 0.346\lambda$	15	3.5	<0.012	9.95	0.22
[23]	40×40	1.71–3.94	$0.228\lambda \times 0.228\lambda$	25	2.36	<0.4	9.71	0.13
[26]	30×30	3.1–12	$0.31\lambda \times 0.31\lambda$	17	6.2	<0.001	9.9	0.1
Proposed work	20×30	3.1–12	$0.206\lambda \times 0.31\lambda$	25	8	<0.2	9.9	0.25

2. Conclusion

This study presents a quad-port antenna system for ultra-wideband applications. Four modified circular radiating components positioned orthogonally across the substrate and each supplied by a 50-microstrip line make up the planned antenna. By including a defective ground structure with two triangular slots at the top side borders of the ground plane and two square slots in the ground plane's centre, ultra-wideband response is made possible. By restricting the current flow between the antenna components through orthogonal designs, interport isolation up to 25 dB is accomplished. Each antenna element is printed on a conventional FR4 substrate with dimensions of $20 \times 30 \times 1.6\,mm^3$ and a dielectric constant and tangential loss of 4.6 and 0.02, respectively. The suggested antenna has an impedance bandwidth of 10 dB and covers the frequency range of 3.1 to 12 GHz. The suggested antenna has considerable radiation characteristics and a peak gain of up to 8 dBi for the operating frequency. Both the measured and the simulated outcomes agreed with one another extremely well. The ECC < 0.25, DG > 9.9, and 2 3 CCL < 0.2 are within the allowed bounds of variation, which further suggests a strong overall performance in terms of variety.

Data Availability

The data used to support the findings of this study are available from the corresponding author upon request.

Conflicts of Interest

The authors declare that they have no conflicts of interest.

References

[1] D. Haripriya, S. Venkatakiran, and A. Gokulachandar, "UWB-MIMO antenna of high isolation two elements with WLAN single band-notched behavior using roger material," *Materials Today Proceedings*, vol. 62, pp. 1717–1721, 2022.

[2] M. Alibakhshikenari, B. S. Virdee, C. H. See, R. A. Abd-Alhameed, F. Falcone, and E. Limiti, "Surface wave reduction in antenna arrays using metasurface inclusion for MIMO and SAR systems," *Radio Science*, vol. 54, no. 11, pp. 1067–1075, 2019.

[3] V. Puri and H. S. Singh, "Design of isolation improved MIMO antenna design using a meta-surface-based absorber for wireless applications," *Optik International Journal for Light and Electron Optics*, vol. 259, pp. 1–11, 2022.

[4] M. N. Hassan, S. Chu, and S. A. Bashir, "DGS monopole antenna loaded with U-shape stub for UWB MIMO applications," *Microwave and Optical Technology Letters*, vol. 61, pp. 2141–2149, 2019.

[5] H. Jiang, L. M. Si, G. Cheng, and X. Lv, "A wideband closed speed 5G MIMO antenna with mutual coupling reduction using combined decoupling networks," in *Proceedings of the 2019 Conference on Microwave and Millimeter Wave Technology (ICT)*, pp. 1–3, Guangzhou, China, May 2019.

[6] H. J. Adamu, H.-X. Zheng, A. Anas, and S. Zhiwei, "Characteristic mode analysis and design of wideband MIMO antenna consisting of metamaterial unit cell," *Electronics*, vol. 68, no. 8, pp. 1–14, 2019.

[7] L. Shuang, W. Daigiang, C. Yuqing, E. Li, and J. Gong, "A compact dual port UWB MIMO antenna with quadruple band-notched characteristics," *International Journal of Electronics and Communications*, vol. 136, pp. 1–9, 2021.

[8] S. Modak and T. Khan, "A slotted UWB-MIMO antenna with quadruple band-notch characteristics using mushroom EBG structure," *AEU International Journal of Electronics and Communications*, vol. 134, pp. 153673–153676, 2021.

[9] A. Desai, J. Kulkarni, M. M. Kamruzzaman, S. Hubalovsky, H. T. Hsu, and A. A. Ibrahim, "Interconnected CPW fed flexible 4-port MIMO antenna for UWB, X, and Ku band applications," *IEEE Access*, vol. 10, pp. 57641–57654, 2022.

[10] Z. Chen, W. Zhou, and J. Hong, "A miniaturized MIMO antenna with triple band-notched characteristics for UWB applications," *IEEE Access*, vol. 9, pp. 63646–63655, 2021.

[11] B. Yang and S. Qu, "A compact integrated Bluetooth UWB dual-band notch antenna for automotive communications," *AEU International Journal of Electronics and Communications*, vol. 80, pp. 104–113, 2017.

[12] M. I. Hussein, H. Ali, and M. Ouda, "Compact low profile planar elliptical antenna for UWB applications," in *Proceedings of the 2016 10th European Conference on Antennas and Propagation*, pp. 1-2, Davos, Switzerland, April 2016.

[13] J. Tao and Q. Feng, "Compact ultra-wideband MIMO antenna with half slot structure," *IEEE Antennas and Wireless Propagation Letters*, vol. 16, pp. 792–795, 2017.

[14] V. S. D. Rekha, P. Pardhasaradhi, B. T. P. Madhav, and Y. U. Devi, "Dual band-notched orthogonal 4-element MIMO antenna with isolation for UWB applications," *IEEE Access*, vol. 8, pp. 145871–145880, 2020.

[15] N. T. Rakesh, S. Prabhakar, K. K. Binod, and S. Kunal, "Neutralization technique baseband and four-port high isolation MIMO antennas for UWB communication," *International Journal of Electronics and Communications*, vol. 110, pp. 1–10, 2019.

[16] H. T. Chattha, F. Latif, F. A. Tahir, M. U. Khan, and X. Yang, "Small-sized UWB-MIMO antenna with band rejection capability," *IEEE Access*, vol. 7, pp. 121816–121824, 2019.

[17] Y. Faouri, S. Ahmad, S. Naseer et al., "Compact super wideband frequency diversity hexagonal-shaped monopole antenna with switchable rejection band," *IEEE Access*, vol. 10, pp. 42321–42333, 2022.

[18] A. H. Jabire, A. Ghaffar, X. J. Li et al., "Metamaterial based design of compact UWB/MIMO monopoles antenna with characteristic mode analysis," *Applied Sciences*, vol. 11, no. 4, p. 1542, 2021.

[19] A. B. Murtala, K. A. I. Mohamad, and Z. Farid, "A compact triband miniaturized MIMO antenna for WLAN applications," *International Journal of Electronics and Communications*, vol. 136, pp. 1–15, 2021.

[20] M. A. Sufian, N. Hussain, A. Abbas, J. Lee, S. G. Park, and N. Kim, "Mutual coupling reduction of a circularly polarized MIMO antenna using parasitic elements and DGS for V2X communications," *IEEE Access*, vol. 10, pp. 56388–56400, 2022.

[21] P. Pannu and D. K. Sharma, "Miniaturize four-port UWB-MIMO antenna with tri-notched band characteristics," *Microwave and Optical Technology Letters*, vol. 63, no. 5, pp. 1489–1498, 2021.

[22] A. K. Aqeel, A. N. Syed, S. K. Muhammad, and I. Bilal, "Quad-port miniaturized MIMO antenna for UWB 11GHz and 13GHz frequency bands," *International Journal of Electronics and Communications*, vol. 131, pp. 1–7, 2021.

[23] A. Iqbal, A. Smida, and A. J. Alazani, "Wideband circularly polarized MIMO antenna for high data wearable biotelemetric devices," *IEEE Access*, vol. 8, pp. 17935–19944, 2020.

[24] I. Elfergani, A. Iqbal, C. Zebiri et al., "Low profile and closely spaced four-element MIMO antenna for wireless body area networks," *Electronics*, vol. 9, no. 2, p. 258, 2020.

[25] M. A. Abdalla and A. A. Ibrahim, "Design and performance evaluation of metamaterial inspired MIMO antennas for wireless applications," *Wireless Personal Communications*, vol. 95, no. 2, pp. 1001–1017, 2017.

[26] A. H. Jabire, S. Sani, S. Saminu, M. J. Adamu, and M. I. Hussein, "A crossed-polarized four port MIMO antenna for UWB communication," *Heliyon*, vol. 9, no. 1, p. e12710, 2023.